

Figure 3.5: (a) Schematic of the volatile cell set up; (b) a high density of dislocations emerging from the reaction front was revealed in single SnO<sub>2</sub> nanowire.

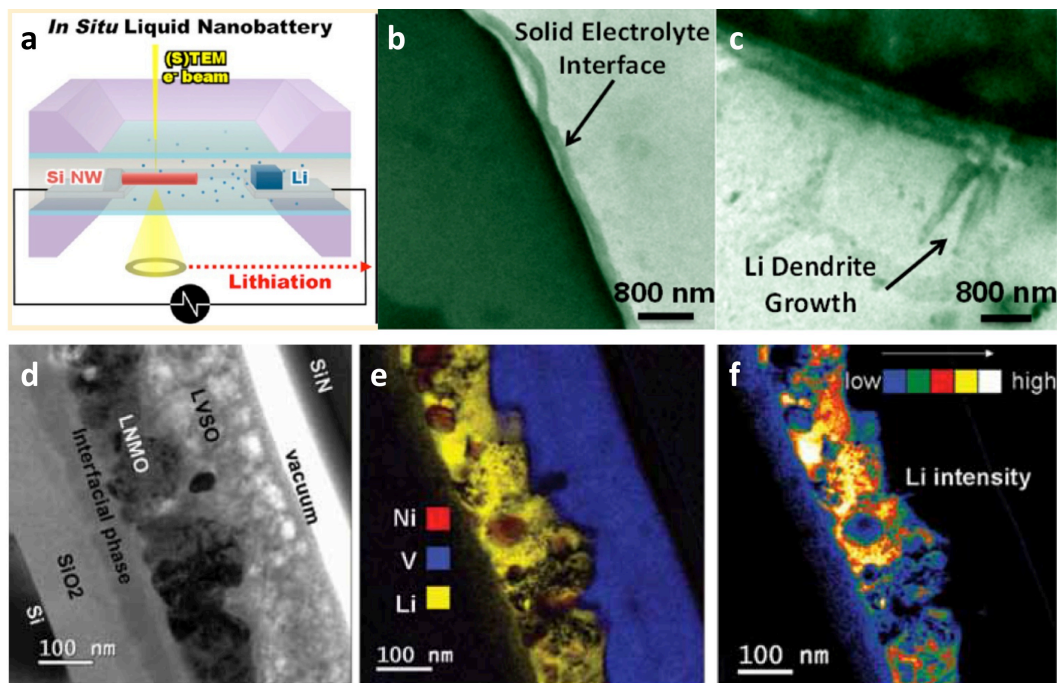


Figure 3.6: (a) Experimental set up of non-volatile cell set up with liquid electrolyte; (b) & (c) in-situ observation of inhomogeneous lithiation, lithium metal dendritic growth and solid-electrolyte interface formation; (d) an example of all-solid-state battery with the configuration of Au (current collector) / SnO<sub>2</sub> (anode) / Li<sub>3.4</sub>V<sub>0.6</sub>Si<sub>0.4</sub>O<sub>4</sub> (electrolyte) / LiNi<sub>0.5</sub>Mn<sub>1.5</sub>O<sub>4</sub> (cathode) / Pt (current collector); (e) & (f) the EELS mapping of Ni, V, Li and Li intensity.

## 4 SURFACE SPIN TRANSITION IN NANO-SIZE STOICHIOMETRIC $\text{LiCoO}_2$ AND ITS APPLICATIONS IN OXYGEN EVOLUTION REACTION / OXYGEN REDUCTION REACTION (OER/ORR) CATALYTIC PROCESS

### 4.1 Electronic Spin Transition in Nano-size Stoichiometric Lithium Cobalt Oxide

#### 4.1.1 Introduction

Lithium cobalt oxide ( $\text{LiCoO}_2$ ) is a compound of great importance, as it has been the most widely used positive electrode material for lithium ion batteries for nearly two decades.  $\text{LiCoO}_2$  adopts the  $\alpha\text{-NaFeO}_2$ -type crystal structure with rhombohedral symmetry (space group R-3m) and  $\text{Li}^+$  and  $\text{Co}^{3+}$  ions sitting in octahedral sites formed by alternating layers of oxygen. Because of such an ordered layered structure,  $\text{Li}^+$  can be reversibly deintercalated and re-intercalated from  $\text{LiCoO}_2$  to  $\text{Li}_{0.5}\text{CoO}_2$  with a high electrochemical potential of up to 4.2V (vs  $\text{Li}^+/\text{Li}$ ). In recent years, it has been demonstrated that ultra fast charge/discharge rate capabilities can be achieved in this compound when nano-scale ( $< 50\text{nm}$ ) particles with morphology optimal for Li intercalation are prepared and tested.<sup>69,70</sup> Okubo et al.<sup>69,71</sup> observed several interesting phenomena associated with their nano-sized  $\text{LiCoO}_2$ : First, lattice parameter expansion is observed in particles less than 20nm; second, the magnetic susceptibility increases dramatically when compared with that of bulk- $\text{LiCoO}_2$ . The authors hypothesized that these phenomena are mainly due to the presence of  $\text{Co}^{2+}$  on the surface of their nano-sized particles,  $\text{Co}^{2+}$  being present in the form of  $\text{Li}_{1-x}\text{Co}^{2+}_x\text{Co}^{3+}_{1-x}\text{O}_2$ , as a consequence of their hydrothermal synthetic process. However, the interpretation of the magnetic data is ambiguous since no direct evidence for the presence of  $\text{Co}^{2+}$  was obtained.<sup>71</sup> Moreover,

Levasseur et al.<sup>72</sup> pointed out that in bulk lithium over-stoichiometric (“Li-excess”) samples, the charge is compensated by oxygen vacancies. This leads to some cobalt ions being in a square based pyramidal site with an intermediate spin (IS) configuration. In this communication we show that, for stoichiometric nano-sized  $\text{LiCoO}_2$ , the anomaly in magnetic susceptibility can similarly be explained by the presence of IS or HS  $\text{Co}^{3+}$ , a phenomenon which alters the lithium (de)intercalation voltage significantly.

## 4.1.2 Methodologies

### 4.1.2.1 Computational Methodology

The DFT + U calculations we adopt here treat core electrons by the projector augmented-wave method<sup>73</sup> as implemented in the Vienna ab initio simulation package (VASP).<sup>74,75</sup> The rotationally invariant approach of the on-site Hubbard U given by Liechtenstein et al.<sup>76</sup> is utilized at the Co sites. The U value,  $U_{\text{eff}} = U - J = 3\text{eV}$ , is chosen similar to a previous study.<sup>77</sup>

All calculations are performed with a plane wave cutoff of 420eV. The four-atom unit cell is used for the bulk calculations. The Brillouin zone is sampled with appropriate k-point mesh to ensure that the total energies are converged within 1meV per formula unit of  $\text{LiCoO}_2$ . For the surface calculation slabs, a similar dense k-point in reciprocal space only parallel to the surface is applied; the surface-plane lattice parameters of slabs are fixed to the bulk values, and only the atomic positions are allowed to relax; Both  $\text{LiCoO}_2$  atomic layer thickness and vacuum thickness are set to be around 20Å, to avoid interactions between slabs.

#### 4.1.2.2 Synthesis of stoichiometric LiCoO<sub>2</sub> nanoparticles.

Chen and Grey have shown previously that a molten salt can be used to synthesize highly stoichiometric LiCoO<sub>2</sub> nanostructures.<sup>70</sup> The particle size and morphology of LiCoO<sub>2</sub> can be controlled by the composition of the molten salts. Higher nitrate concentrations in the eutectic system results in a smaller LiCoO<sub>2</sub> particle size; while higher hydroxides concentration results in a larger particle size or in 3D nanostructures. In this work, the previously reported molten salt method was modified in order to synthesize stoichiometric LiCoO<sub>2</sub> with very fine and tunable particle sizes, e.g. from ~10 nanometers to a few tens of nanometers. Nano Co(OH)<sub>2</sub> was used as the cobalt source instead of cobalt nitrate. It was synthesized by a precipitation method: 1 M Co(NO<sub>3</sub>)<sub>2</sub>·6(H<sub>2</sub>O) solution was slowly added into a 0.1 M LiOH solution under 400 rpm magnetic stirring. LiOH was 5% excess to the stoichiometric amount. The brown precipitate (Co(OH)<sub>2</sub>) was filtered and washed by distilled water and methanol several times and dried in a vacuum oven at 60°C overnight. In a typical synthesis of stoichiometric nano-LiCoO<sub>2</sub>, a 10-gram mixture containing lithium and potassium salts (various molar ratios were used depending on the desired size of LiCoO<sub>2</sub> (see Table 4.1)) was heated in a PTFE crucible at 200°C (uniform heating was achieved by placing the crucible in an oil bath), to form a clear flux. Then 200 mg of the as-prepared Co(OH)<sub>2</sub> powder was then added into the mixture under magnetic stirring (600 rpm). The temperature of the flux was kept at 200°C for a certain period of time depending on the desired particle size (see Table 4.1). The crucible was then taken out of the oil bath and quenched with distilled water. The solid product was separated from the salts by filtration,

washed with distilled water, and then dried at 90°C overnight in a vacuum oven. The type and ratio of the Li and K salts in addition to the reaction times were varied to control the particle size of the LiCoO<sub>2</sub> products, as listed in Table 4.1. Crystallite size was estimated from the line broadening in the XRD patterns by using the Scherrer equation.<sup>78</sup> Fits were conducted on 9 peaks and averaged to give the calculated crystallite size.

#### **4.1.2.3 XRD Instrumentation and Lattice Parameters**

X-ray diffraction data was collected using a Rigaku Miniflex II Bragg-Brentano diffractometer, which features a high-power rotating anode X-ray generator operating at 13kW. The X-ray source is a Cr target. The goniometer is a 185mm radius horizontal-circle with a diffracted-beam graphite monochromator and scintillation detector. The data was collected at a step size of 0.02° every 10s.

#### **4.1.2.4 XPS Instrumentation**

Nano-sized LiCoO<sub>2</sub> samples were prepared by pressing each powder onto a strip of double-sided adhesive tape followed by mounting onto the sample holder for XPS analysis. Room temperature XPS was performed on a Thermo Scientific K-alpha microprobe with a focused monochromatic Al K<sub>α</sub> X-ray (1486.6 eV) source. A hemispherical analyzer was equipped, with an incident X-ray beam 45° off normal to the sample while the X-ray photoelectron detector was normal to the sample, and the chamber pressure was kept at < 10<sup>-10</sup> Torr for all measurements. Charge compensation was employed during data collection (1 eV, 20 μA electrons) and binding energies of the photoelectron were corrected to the aliphatic hydrocarbon C 1s peak at 284.6 eV.

#### 4.1.2.5 $^7\text{Li}$ NMR

$^7\text{Li}$  NMR data were collected using 1.8 mm probe made by Dr, Ago Samoson. A spin echo pulse sequence was used ( $90^\circ$ - t - $180^\circ$ - t -acq, where t is one spinning rotor period, acq is the acquisition time, and  $90^\circ$  and  $180^\circ$  radio frequency pulse durations are about 1.6 and 3.2 ms, respectively) to ensure the observation of the very broad signals which could be missing in a single pulse experiment due to the receiver dead time. The isotropic shifts of the broad peaks corresponding with negative hyperfine shifts were determined by comparing spectra collected at different spinning speeds. Quantification of the fraction of the peaks with negative hyperfine shifts was obtained by curve fitting the spectra.

#### 4.1.2.6 Fitting Equation for the Curie Constant

$$C = p \frac{N_A}{3k_B} n(n+2)\mu_B^2 = 1.25pn(n+2)$$

Theoretical Curie constant

p = number of magnetic species per mole

n = the number of unpaired electrons in the magnetic species (n=2 for  $\text{Co}^{3+}$  mid spin)

$N_A$  = Avogadro's number

$k_B$  = Boltzmann constant

$\mu_B$  = Bohr magneton

### 4.1.3 Results and Discussions

The surface energies of  $\text{LiCoO}_2$  were calculated from first principles with the Hubbard U correction on the generalized gradient approximation (GGA+U) to the density functional theory (DFT). The results are listed in Table 4.3. We find that the surface energies are minimized when the surface  $\text{Co}^{3+}$  ions are either in the intermediate (IS) or high spin (HS) state depending on the crystallographic orientation. This change in the electronic spin state on the surface can be rationalized by a change in the surface Co crystal field due to the missing Co-O bonds.

$\text{LiCoO}_2$  particles are typically dominated by the  $\{001\}$  surface, however this surface is not active for Li (de)intercalation. Therefore, we focus on studying the  $\{104\}$  and  $\{110\}$  surfaces, which are the two lowest energy non-polar surfaces identified by previous work.<sup>79</sup> Figure 4.1a shows the  $\{104\}$  surface of  $\text{LiCoO}_2$ , which represents a major, low energy surface for  $\text{LiCoO}_2$ ; this surface slices through the Co, O and Li planes and is expected to be involved in the (de)intercalation process. This represents the  $\{100\}$  surface of the NaCl lattice from which the ordered rocksalt  $\text{LiCoO}_2$  is derived. In the bulk, and on the  $\{001\}$  surface, octahedrally coordinated  $\text{Co}^{3+}$  ions are in the low spin (LS) state and do not have unpaired electrons. On the  $\{104\}$  surface, however, the  $\text{Co}^{3+}$  ions are coordinated by five oxygen ions, resulting in a square pyramidal configuration. The surface energy is then lowered significantly when going from the LS configuration ( $1118\text{mJ/m}^2$ ) to the IS ( $312\text{mJ/m}^2$ ). Figure 4.1b depicts the  $\{110\}$  surface of  $\text{LiCoO}_2$ . In this orientation, the  $\text{Co}^{3+}$  ions on the surface are coordinated by four oxygen ions with a pseudo-tetrahedral configuration. The surface energy is minimized from  $2227\text{mJ/m}^2$  (LS) to  $1241\text{mJ/m}^2$  (HS). The details of the crystal field splitting of  $3d$  orbitals and the corresponding energy levels of bulk and surface cobalt ions are shown in Figure 4.1c. A

square pyramidal crystal field breaks the degeneracy of both the  $t_{2g}$  and  $e_g$  orbitals observed for octahedral symmetry, since the missing O ion along the z-direction reduces the repulsion between  $2p$  electrons and  $3d$  electrons in orbitals pointing towards or closer to the z-axis. A pseudo-tetrahedral crystal field with two missing bonds in the  $xy$  plane leads to lower energies for the  $3d_{xy}$  and  $3d_{x^2-y^2}$  orbitals. A charge density plot, which represents the difference in up and down spins, of the  $\{104\}$  surface clearly show the unpaired electrons as compared to the case of  $\text{Co}^{3+}$  (LS) in the bulk of  $\text{LiCoO}_2$ . (See Figure 4.2a and 4.2b) The first principles calculations reveal that both the  $\{104\}$  and  $\{110\}$  surfaces with optimized Co coordination environments and electronic states expand normal to the surface, the displacement being on the order of 0.1-0.2Å. It is important to point out that such changes in electronic spin states are also seen in first principles simulations of surfaces of  $\text{CoO}$  and  $\text{Co}_2\text{O}_3$ , as well as  $\text{LiNiO}_2$ .

To validate the hypothesis that the  $\text{Co}^{3+}$  on the surface is in an intermediate spin state by experimental spectroscopic techniques, stoichiometric  $\text{LiCoO}_2$  samples with extremely small particle sizes (thus very large surface areas) provide the best opportunities. However, it is difficult to make stoichiometric nanoparticles of  $\text{LiCoO}_2$  by conventional solid state or hydrothermal methods.<sup>80</sup> Okubo et al. reported samples with small particle sizes (8 to 32 nm), but the samples are most likely over-stoichiometric, i.e.,  $\text{Li}_{1+x}\text{CoO}_2$ .<sup>69</sup> By contrast, the molten salt method reported earlier<sup>70</sup> represents a much better approach to prepare stoichiometric  $\text{LiCoO}_2$  nanoparticles. In this work, stoichiometric  $\text{LiCoO}_2$  with very small particle sizes (10nm, 16nm, 20nm, 30nm and 40nm) were synthesized by using a modified molten salt method based on the previously reported method. We observed expansion of the lattice parameters from Rietveld analysis